

# Force generation by skeletal muscle is controlled by mechanosensing in myosin filaments

Marco Linari<sup>1,2</sup>, Elisabetta Brunello<sup>1†</sup>, Massimo Reconditi<sup>1,2</sup>, Luca Fusi<sup>3</sup>, Marco Caremani<sup>1</sup>, Theyencheri Narayanan<sup>4</sup>, Gabriella Piazzesi<sup>1</sup>, Vincenzo Lombardi<sup>1</sup> & Malcolm Irving<sup>3</sup>

**Contraction of both skeletal muscle and the heart is thought to be controlled by a calcium-dependent structural change in the actin-containing thin filaments, which permits the binding of myosin motors from the neighbouring thick filaments to drive filament sliding<sup>1–3</sup>. Here we show by synchrotron small-angle X-ray diffraction of frog (*Rana temporaria*) single skeletal muscle cells that, although the well-known thin-filament mechanism is sufficient for regulation of muscle shortening against low load, force generation against high load requires a second permissive step linked to a change in the structure of the thick filament. The resting (switched ‘OFF’) structure of the thick filament is characterized by helical tracks of myosin motors on the filament surface and a short backbone periodicity<sup>2,4,5</sup>. This OFF structure is almost completely preserved during low-load shortening, which is driven by a small fraction of constitutively active (switched ‘ON’) myosin motors outside thick-filament control. At higher load, these motors generate sufficient thick-filament stress to trigger the transition to its long-periodicity ON structure, unlocking the major population of motors required for high-load contraction. This concept of the thick filament as a regulatory mechanosensor provides a novel explanation for the dynamic and energetic properties of skeletal muscle. A similar mechanism probably operates in the heart.**

Muscle contraction is driven by the relative sliding of two sets of overlapping filaments, the myosin-containing thick filaments and the actin-containing thin filaments, coupled to ATP hydrolysis. In the widely accepted model of skeletal muscle regulation, excitation of a motor nerve causes release of calcium ions within the muscle cell that bind to troponin in the thin filaments, triggering a structural change that allows binding of the myosin motor domains of the thick filaments<sup>1</sup>. In resting muscle, however, the myosin motors are packed into helical tracks on the surface of the thick filaments<sup>2–6</sup>, making them unavailable for actin binding or ATP hydrolysis<sup>7</sup>, implying the presence of a second thick-filament-based switch for contraction. The fact that the length and axial periodicity of the thick filaments increase slightly on muscle activation<sup>2,4,8,9</sup> or when resting muscle is stretched<sup>4,8–10</sup> suggests that the thick-filament switch might be mechanical, and that unpacking of the myosin motors on muscle activation might be triggered by thick-filament stress.

We used synchrotron small-angle X-ray diffraction of isolated muscle cells to test this idea (Fig. 1, see Methods). When an isolated muscle cell is activated at constant length (Fig. 1a, thick lines), force and filament stress start to increase about 10 ms after the start of stimulation (the latent period), when activation of the troponin complex in the thin filaments is already maximal<sup>3,11,12</sup>. To determine the effect of thick-filament stress on its structure during activation, we imposed rapid shortening of about 5% fibre length (Fig. 1a, thin

line in left section) to delay development of force and filament stress for about 20 ms.

The OFF structure of the thick filament, seen in resting muscle, has a characteristic X-ray signature. The three-stranded helical arrangement of the myosin motors on the filament surface produces a series of layer-line reflections (of which the first order is called ML1) that are orders of a fundamental axial periodicity of about 43 nm, and corresponding axial reflections (of which the first order is called M1)<sup>2</sup>. Two other thick-filament components, myosin binding protein-C (MyBP-C) and titin follow the ~43-nm periodicity, and MyBP-C makes a substantial contribution to the M1 (ref. 13). The M2 reflection signals systematic perturbations in the helical arrangement. The M3, from the axial repeat of the motors, has a periodicity ( $S_{M3}$ ) of 14.34 nm in the OFF state, and the M6, dominated by the periodic mass distribution in the thick-filament backbone<sup>14,15</sup>, has a periodicity ( $S_{M6}$ ) of 7.17 nm. The axial reflections exhibit multiple peaks associated with X-ray interference between the two halves of each filament<sup>8,9,14,15</sup>.

These X-ray signals show that the thick filament remains OFF when its stress is abolished by applying rapid shortening during early activation. The intensities of the ML1, M1, M2, M3 and M6 reflections during such shortening (Fig. 1b–f, blue) are the same as those at rest (green), as are the characteristic OFF periodicities  $S_{M3}$  and  $S_{M6}$ . This behaviour is in marked contrast with the ON state at maximum isometric force ( $T_0$ ) reached after 200 ms of activation (Fig. 1a, red rectangle), in which ML1 is replaced by a much weaker actin-based reflection AL1 (Fig. 1b, red), M2 is absent (Fig. 1d), M3 moves to a periodicity of 14.57 nm (Fig. 1e) and  $S_{M6}$  increases to 7.29 nm (Fig. 1f).  $S_{M6}$  and the intensity of the M2 reflection,  $I_{M2}$ , are particularly sensitive to thick-filament stress. Thus, if the force is allowed to rise to about 0.1  $T_0$  at the same time as the zero-stress data were recorded (Fig. 1a, orange rectangle),  $I_{M2}$  and  $S_{M6}$  (Fig. 1d, f, orange) have already started to move towards their fully ON values (red)<sup>16</sup> (see also Extended Data Fig. 1). These results show that the OFF structure of the thick filament is fully preserved early in the activation process, when the intracellular calcium concentration is maximal, provided that thick-filament stress is abolished. Muscle can generate shortening at the maximum velocity with most of its myosin motors switched OFF, but a small stress (0.1  $T_0$ ) is sufficient to trigger an increase in filament periodicity and exit from the OFF conformation, consistent with the mechanosensing hypothesis.

To test this idea further, we allowed the thick filament to attain its fully ON structure at force  $T_0$ , then imposed rapid shortening of 10% fibre length to hold force at zero for about 40 ms (Fig. 1a, right section). The ML1 reflection signalling the OFF structure partially recovered (Fig. 1b, purple), and its periodicity returned completely to the OFF value. The M2 reflection, which is absent at  $T_0$ , reappeared (Fig. 1d, purple). The periodicity of the M3 reflection recovered

<sup>1</sup>Laboratory of Physiology, Department of Biology, Università di Firenze, Sesto Fiorentino, 50019 Florence, Italy. <sup>2</sup>Consorzio Nazionale Interuniversitario per le Scienze Fisiche della Materia, UdR Firenze, Sesto Fiorentino, 50019 Florence, Italy. <sup>3</sup>Randall Division and BHF Centre for Research Excellence, King's College London, London SE1 1UL, UK. <sup>4</sup>European Synchrotron Radiation Facility, BP220, F-38043 Grenoble, France. <sup>†</sup>Present address: Randall Division and BHF Centre for Research Excellence, King's College London, London SE1 1UL, UK.

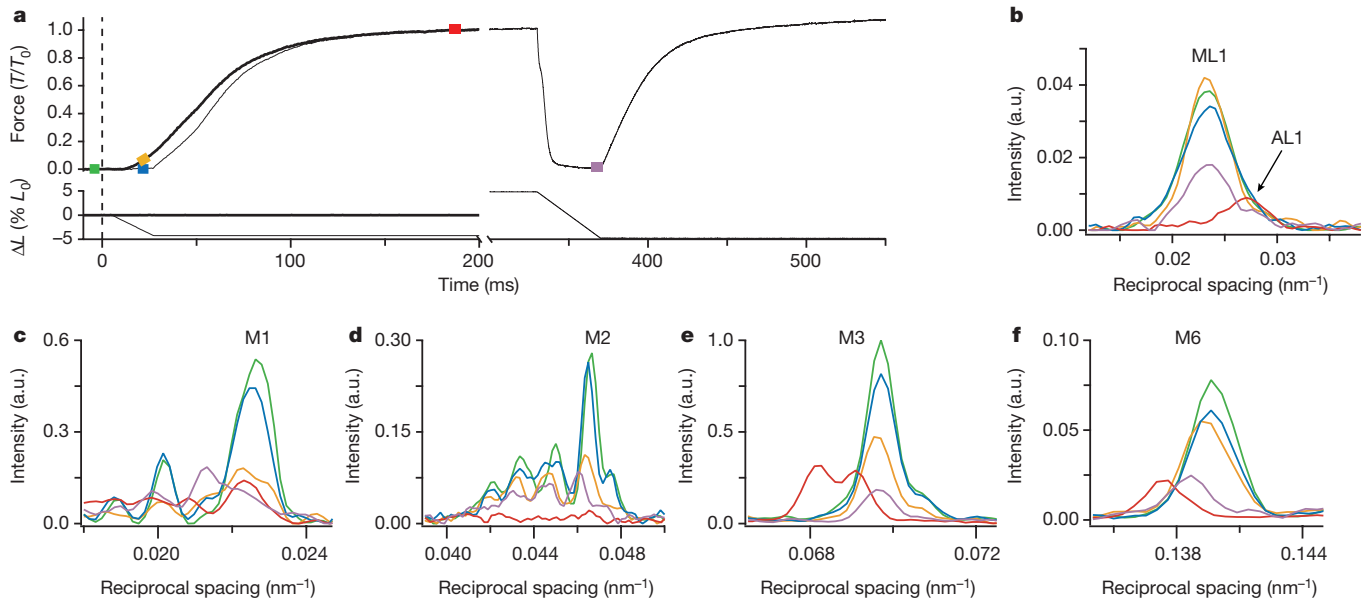


**Figure 1 | X-ray reflections associated with thick-filament structure in isolated skeletal muscle fibres depend on the external load during activation.** **a**, Force and fibre length change ( $\Delta L$ , expressed as a percentage of initial fibre length (%  $L_0$ )) following stimulation starting at time zero (vertical dashed line). X-ray time exposures are denoted by coloured rectangles: green, resting; blue, shortening during early activation; red, maximum isometric force ( $T_0$ ); orange, low isometric force ( $0.1 T_0$ );

purple, shortening from the maximum isometric force. **b**, Intensity profile of the ML1 and AL1 layer-line reflections from the myosin and actin helices, respectively. **c–f**, Meridional intensity profiles for the M1, M2, M3 and M6 reflections, respectively. Colours in **b–f** relate to protocols (coloured rectangles) in **a**; X-ray data added from three (green, yellow, blue) or two (red, purple) fibres with 3 m (**b, f**) or 10 m (**c–e**) camera length. a.u., arbitrary units.

completely to its resting value of 14.34 nm (Fig. 1e, purple), and the double-peak interference effect characteristic of full activation was lost. The filament backbone periodicity ( $S_{M6}$ ; Fig. 1f) partially recovered from 7.29 nm at  $T_0$  (red) to 7.22 nm (purple).

The fully ON thick filament can therefore be switched OFF by decreasing filament stress to zero, further supporting the mechanosensing hypothesis. The extent of switching OFF, measured by the intensities of the ML1 and M2 reflections ( $I_{ML1}$  and  $I_{M2}$ ; Fig. 2a, b) or  $S_{M6}$  (Fig. 2c), increases with a half-time of  $\sim 20$  ms during the zero-stress period. This is much slower than the decrease in force (continuous line). This is much slower than the decrease in force (continuous line) or the fraction of myosin motors attached to actin, estimated from sarcomere stiffness, which has a half-time of  $\sim 3$  ms (Extended Data Fig. 2)<sup>17</sup>. Thus the rate of switching OFF the thick filament at zero force is limited by a transition in the detached myosin motors. Biochemical kinetic modelling suggests that the rate-limiting step is a stress-sensitive isomerization between states with bound ATP hydrolysis products (see Supplementary Discussion and Extended Data Fig. 2).

When force was allowed to redevelop after 40 ms at zero thick-filament stress, the filament returned to a fully ON structure, as measured by  $I_{ML1}$ ,  $I_{M2}$  and  $S_{M6}$ , again with a half-time of  $\sim 20$  ms, similar to that of force redevelopment (Fig. 2). Recovery of the intensity and interference fine structure of the M3 reflection had an  $\sim 10$ -ms lag, corresponding to force generation by disordered motors formed at zero stress (see Supplementary Discussion and Extended Data Fig. 3). The temporal correspondence between force redevelopment and recovery of the ON structure of the thick filament suggests that the rate of force generation in muscle is controlled by the availability of ON motors, and therefore by thick-filament structure.

To test the generality of this conclusion, we compared isometric force development after different periods of zero-force shortening to that at the start of calcium activation, in which force development starts from the end of the  $\sim 10$ -ms latent period (Fig. 3a, solid black line). The later time course of force development is well fit by an exponential (dashed black line) with a time constant ( $\tau$ ) of 34 ms (Fig. 3b, black circle), and a delay ( $\Delta t$ ) of 21 ms after the latent period (Fig. 3c). Force development after 20 ms of zero-force

shortening at the start of electrical stimulation (light blue) has the same  $\tau$  and a slightly smaller  $\Delta t$  (15 ms, measured from the end of shortening). In both cases, force develops from an almost fully OFF state of the thick filament, with  $S_{M6}$  close to its resting value (Fig. 3d). In contrast, force development after 40 ms of zero-force shortening from  $T_0$ , starting with the thick filament about half-OFF as

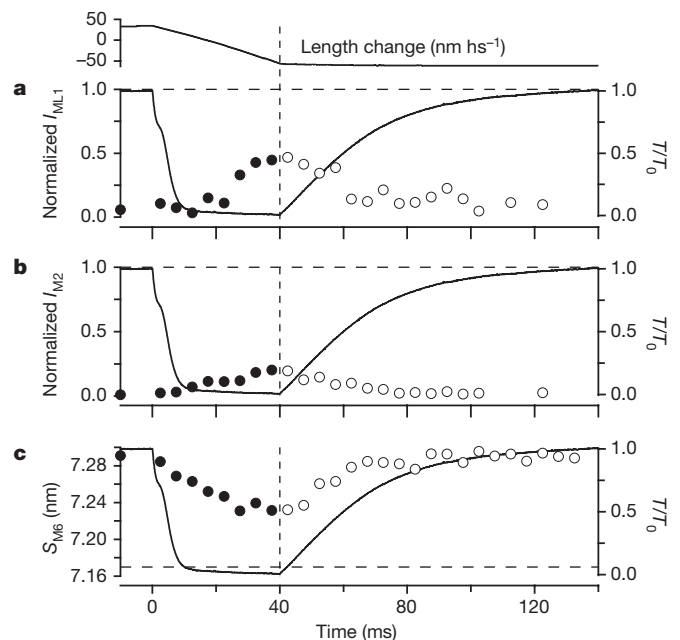


**Figure 2 | The OFF structure of the thick filament is transiently restored when the load on a fully active muscle fibre is removed.** Top, sarcomere length change, shown in nanometres per half-sarcomere (hs). **a–c**, Changes in  $I_{ML1}$  (**a**),  $I_{M2}$  (**b**) and  $S_{M6}$  (**c**) (circles) and force (solid line). Horizontal dashed lines, resting value of X-ray parameter; vertical dashed lines, time of end of shortening. X-ray data in **a** and **b** added from three fibres, those in **c** from two fibres. Filled/open circles denote data before/after the end of shortening.

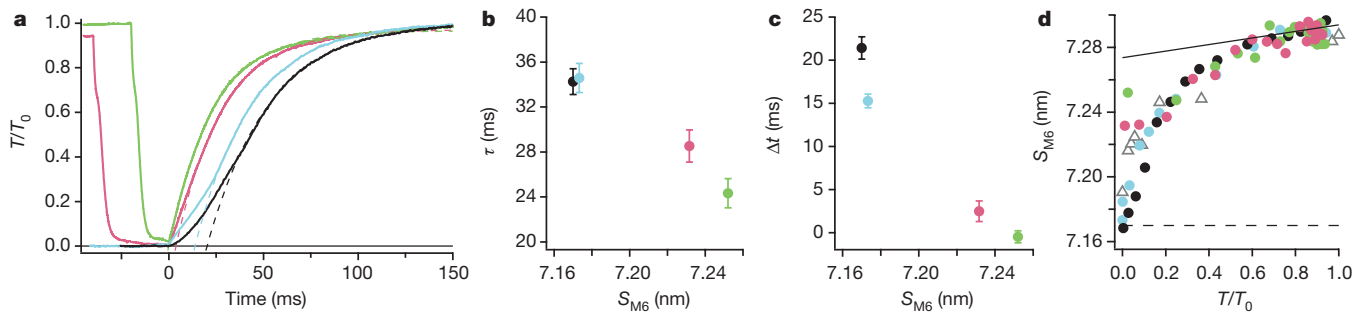


**Figure 3 | The time course of force development is controlled by the regulatory state of the thick filament.** **a**, Time course of isometric force development following stimulation (black solid line); after 5% shortening from the latent period (light blue); and after 5% (green) or 10% (pink) shortening from the tetanus plateau, superimposed at the start of the force rise. **b, c**, Time constant ( $\tau$ ) (**b**) and delay ( $\Delta t$ ) (**c**) from exponential fits in **a** (mean  $\pm$  s.e.m.;  $n = 5$  fibres, except pink data ( $n = 3$ )) plotted against

$S_{M6}$  just before the start of force development. **d**, Instantaneous  $S_{M6}$ –force relationship for the four protocols in **a** (circles; data added from three fibres except pink and green ( $n = 2$ )). Continuous line, instantaneous filament compliance<sup>23</sup>; dashed line, resting value. Triangles, steady-state activation of demembrated mammalian muscle fibres at different free calcium concentrations (data from four fibre bundles). Colours in **b–d** denote protocols in **a**.

measured by  $S_{M6}$  (pink), is much faster ( $\tau = 28$  ms;  $\Delta t = 2$  ms). After only 20 ms of zero-force shortening from  $T_0$  (green), force development starts from a higher  $S_{M6}$  (Fig. 2c) and is even faster ( $\tau = 24$  ms;  $\Delta t = 0$  ms).

This correlation between the regulatory state of the thick filament and the kinetics of force development strongly supports the conclusion that the time course of force development is determined by availability of ON motors. For forces larger than  $0.1 T_0$ , there is a unique nonlinear relationship between  $S_{M6}$  and force in all four protocols (Fig. 3d). As the high-force part of this relationship is due to filament compliance (Fig. 3d, solid line), the thick filament may be considered to be fully ON for forces greater than about  $0.5 T_0$ . This relationship between thick-filament periodicity and stress is not limited to the protocols and muscle preparation used here; essentially the same relationship was observed when filament stress was modulated by varying the free calcium concentration in demembrated fibres from mammalian muscle in steady-state fixed-length conditions (Fig. 3d, triangles).

The results presented above lead to a novel dual-filament concept of muscle regulation (Fig. 4). If the external load is zero when the thin filaments are activated by calcium (Fig. 4b), muscle shortens at its maximum velocity, which is the same at the end of the latent period and during full activation<sup>16,18</sup> (Fig. 1). Less than 5% of the myosin motors are required to drive unloaded shortening<sup>17</sup>, and we propose that these motors are constitutively ON (Fig. 4, dark green ellipses). Unloaded shortening is therefore solely controlled by the regulatory state of the thin filament, and can be mobilized immediately after calcium release at low metabolic cost. The constitutively ON motors that drive unloaded shortening may be in the less ordered regions of the thick filament where MyBP-C is absent<sup>6,19</sup>, or a subset of the motors in the MyBP-C-containing region (the C zone). In either case, in the presence of an external load, the constitutively ON motors generate stress in the thick filament (Fig. 4c), releasing the remaining motors from the OFF state, and allowing development of the full isometric force  $T_0$ .

The molecular interactions stabilizing the OFF state of the myosin motors on the surface of the thick filaments in vertebrate skeletal muscle are not well understood, but may involve the motors binding to the myosin tail<sup>20</sup>, MyBP-C<sup>21</sup> and titin<sup>22</sup>, which all share the  $\sim 43$ -nm periodicity in the C zone. We postulate that these interactions stabilize the  $14.34 = 2 \times 7.17$ -nm axial periodicity of the helical OFF state (Fig. 4a, b), and that in their absence the thick filament reverts to the longer 14.57-nm periodicity (Fig. 4c), determined by the packing of myosin tails in its backbone. Filament stress controls the transition between these two states by breaking the molecular interactions that stabilize the short or OFF state and decreasing the relative free energy of the long or ON state.

This thick-filament mechanosensing mechanism for the regulation of force generation in skeletal muscle has several wider implications. The OFF state of the thick filament inhibits ATP utilization by the great majority of the myosin motors, inducing the ‘super-relaxed’ state<sup>7</sup>, but the small fraction of constitutively ON motors allows the muscle to respond immediately to calcium activation when the external load is low. At high load, stress-dependent activation of the thick filament initiates a positive feedback loop, mobilizing more motors that generate more force to further increase thick-filament stress. This phase of motor unpacking dominates the initial accelerating phase of force development after calcium activation (Fig. 3a), consistent with the dependence of the kinetics of force development on thick-filament structure (Fig. 3b, c). Thus, the physiological rate of force development is determined by the time course of thick-filament activation. The classical force–velocity relationship of skeletal muscle, the fundamental determinant of its dynamic performance and efficiency, also has a new molecular explanation in terms of thick-filament mechanosensing. Finally, as thick-filament structure and protein composition are essentially the same in heart and skeletal muscle, thick-filament mechanosensing may also be a

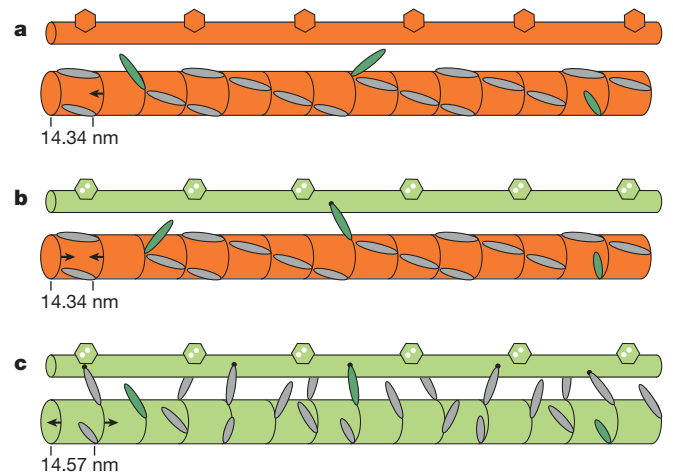


**Figure 4 | Dual-filament regulation in skeletal muscle.** **a**, Resting muscle. **b, c**, Calcium activation at low and high load, respectively. Thin (top structure) and thick (bottom structure) filaments may be OFF (orange) or ON (green). The OFF thick filament has a compressed 14.34-nm backbone periodicity (arrows); most myosin motors (grey) form helical tracks, but others (dark green) are constitutively ON. When the thin filament is activated by calcium binding to troponin (hexagons), the constitutively ON motors drive filament sliding at low load (**b**). At high load (**c**), force generated by constitutively ON motors switches the thick filament ON (14.57-nm periodicity), releasing the remaining motors.

fundamental component of the regulation of contractility in the heart, opening the possibility of new approaches for therapeutic control of cardiac output.

**Online Content** Methods, along with any additional Extended Data display items and Source Data, are available in the online version of the paper; references unique to these sections appear only in the online paper.

**Received 23 April; accepted 21 September 2015.**

**Published online 11 November 2015.**

- Gordon, A. M., Homsher, E. & Regnier, M. Regulation of contraction in striated muscle. *Physiol. Rev.* **80**, 853–924 (2000).
- Huxley, H. E. & Brown, W. The low-angle X-ray diagram of vertebrate striated muscle and its behaviour during contraction and rigor. *J. Mol. Biol.* **30**, 383–434 (1967).
- Reconditi, M. *et al.* Motion of myosin head domains during activation and force development in skeletal muscle. *Proc. Natl Acad. Sci. USA* **108**, 7236–7240 (2011).
- Haselgrove, J. C. X-ray evidence for conformational changes in the myosin filaments of vertebrate striated muscle. *J. Mol. Biol.* **92**, 113–143 (1975).
- Woodhead, J. L. *et al.* Atomic model of a myosin filament in the relaxed state. *Nature* **436**, 1195–1199 (2005).
- Luther, P. K. *et al.* Direct visualization of myosin-binding protein C bridging myosin and actin filaments in intact muscle. *Proc. Natl Acad. Sci. USA* **108**, 11423–11428 (2011).
- Stewart, M. A., Franks-Skiba, K., Chen, S. & Cooke, R. Myosin ATP turnover rate is a mechanism involved in thermogenesis in resting skeletal muscle fibers. *Proc. Natl Acad. Sci. USA* **107**, 430–435 (2010).
- Linari, M. *et al.* Interference fine structure and sarcomere length dependence of the axial x-ray pattern from active single muscle fibers. *Proc. Natl Acad. Sci. USA* **97**, 7226–7231 (2000).
- Reconditi, M. *et al.* Sarcomere-length dependence of myosin filament structure in skeletal muscle fibres of the frog. *J. Physiol. (Lond.)* **592**, 1119–1137 (2014).
- Irving, T. *et al.* Thick-filament strain and interfilament spacing in passive muscle: effect of titin-based passive tension. *Biophys. J.* **100**, 1499–1508 (2011).
- Caputo, C., Edman, K. A., Lou, F. & Sun, Y. B. Variation in myoplasmic Ca<sup>2+</sup> concentration during contraction and relaxation studied by the indicator fluo-3 in frog muscle fibres. *J. Physiol. (Lond.)* **478**, 137–148 (1994).
- Yagi, N. An X-ray diffraction study on early structural changes in skeletal muscle contraction. *Biophys. J.* **84**, 1093–1102 (2003).
- Rome, E., Offer, G. & Pepe, F. A. X-ray diffraction of muscle labelled with antibody to C-protein. *Nat. New Biol.* **244**, 152–154 (1973).
- Reconditi, M. *et al.* The myosin motor in muscle generates a smaller and slower working stroke at higher load. *Nature* **428**, 578–581 (2004).
- Huxley, H., Reconditi, M., Stewart, A. & Irving, T. X-ray interference studies of crossbridge action in muscle contraction: evidence from quick releases. *J. Mol. Biol.* **363**, 743–761 (2006).
- Brunello, E. *et al.* Structural changes in the myosin filament and cross-bridges during active force development in single intact frog muscle fibres: stiffness and X-ray diffraction measurements. *J. Physiol. (Lond.)* **577**, 971–984 (2006).
- Piazzesi, G. *et al.* Skeletal muscle performance determined by modulation of number of myosin motors rather than motor force or stroke size. *Cell* **131**, 784–795 (2007).
- Lombardi, V. & Menchetti, G. The maximum velocity of shortening during the early phases of the contraction in frog single muscle fibres. *J. Muscle Res. Cell Motil.* **5**, 503–513 (1984).
- Bennett, P. M. & Gautel, M. Titin domain patterns correlate with the axial disposition of myosin at the end of the thick filament. *J. Mol. Biol.* **259**, 896–903 (1996).
- Jung, H. S., Komatsu, S., Ikebe, M. & Craig, R. Head-head and head-tail interaction: a general mechanism for switching off myosin II activity in cells. *Mol. Biol. Cell* **19**, 3234–3242 (2008).
- Pfuhl, M. & Gautel, M. Structure, interactions and function of the N-terminus of cardiac myosin binding protein C (MyBP-C): who does what, with what, and to whom? *J. Muscle Res. Cell Motil.* **33**, 83–94 (2012).
- Muhle-Goll, C. *et al.* Structural and functional studies of titin's fn3 modules reveal conserved surface patterns and binding to myosin S1—a possible role in the Frank-Starling mechanism of the heart. *J. Mol. Biol.* **313**, 431–447 (2001).
- Brunello, E. *et al.* The contributions of filaments and cross-bridges to sarcomere compliance in skeletal muscle. *J. Physiol. (Lond.)* **592**, 3881–3899 (2014).

**Supplementary Information** is available in the online version of the paper.

**Acknowledgements** We thank M. Dolfi and J. Gorini for electronic and mechanical engineering support and P. Panine for assistance at the beamline. We thank ESRF for beamtime, and Ente Cassa di Risparmio di Firenze 2010.1402, FIRB-Futuro in Ricerca project RBFRO8JAMZ, MIUR-PRIN project 2010R8JK2X (Italy), MRC (UK) and ESRF for financial support.

**Author Contributions** M.L., E.B., M.R., L.F., M.C., G.P., V.L. and M.I. contributed to the conception and design of the experiments, the collection, analysis and interpretation of data, and drafting or critical revision of the article. T.N. contributed to data collection and analysis.

**Additional Information** Reprints and permissions information is available at [www.nature.com/reprints](http://www.nature.com/reprints). The authors declare no competing financial interests. Readers are welcome to comment on the online version of the paper. Correspondence and requests for materials should be addressed to V.L. ([vincenzo.lombardi@unifi.it](mailto:vincenzo.lombardi@unifi.it)).

## METHODS

No statistical methods were used to predetermine sample size.

**Muscle fibres and experimental protocol.** Adult male frogs (*Rana temporaria*, 3–6 years old) were killed by decapitation and destruction of the brain and spinal cord, as approved by the Ethical Committee for the animal experimentation of the University of Florence, following European Community Council Directive 86/609/EEC. Frogs were chosen at random for each experiment from the available batch, and each experiment was performed using protocols with internal controls on the same frog muscle fibre to minimize systematic errors owing to inter-animal variation. Single fibres ~6 mm long were dissected from the tibialis anterior muscle and mounted via aluminium foil clips attached to the tendons in a trough containing Ringer's solution (115 mM NaCl, 2.5 mM KCl, 1.8 mM CaCl<sub>2</sub> and 3 mM phosphate buffer, pH 7.1). A pair of mica windows was positioned close to the fibre, about 600 µm apart, to minimize the X-ray path in solution. Sarcomere length, fibre length and cross-sectional area were measured with a 40× water immersion objective and a 25× eyepiece. Resting sarcomere length was set to  $2.14 \pm 0.02$  µm (mean ± s.d.). Force was measured with a capacitance transducer<sup>24</sup>. The length of a population of sarcomeres in a 1–2 mm segment of the fibre was measured with a striation follower<sup>25</sup> in control tetani before mounting the fibre vertically at the beamline. Trains of stimuli of alternating polarity, at a frequency of 20–24 Hz, were delivered every 4 min at 4 °C via platinum electrodes on the top and bottom edges of the opposing windows to elicit fused tetani lasting 390–550 ms. A steady shortening of  $5.0 \pm 0.2\%$  (mean ± s.e.m.,  $n = 8$ ) of the initial fibre length ( $L_0$ ) at the maximum velocity of shortening ( $V_0$ ) was applied either 5 ms after the first stimulus, to keep the force at zero, or at the plateau of the isometric tetanus ( $T_0$ ). After the imposed shortening, the isometric force developed at the new sarcomere length (Figs 1a and 3a). Alternatively, the fibre was slowly stretched at rest by 5%  $L_0$  and a steady shortening of 10%  $L_0$  ( $10.0 \pm 0.3\%$ ,  $n = 5$ ) at  $V_0$  was imposed at the plateau of an isometric tetanus. This protocol minimized sarcomere length differences at the end of ramp shortening between the various protocols used for X-ray measurements.  $V_0$  measured with the striation follower was  $2.7 \pm 0.2$  µm s<sup>-1</sup> per half-sarcomere (mean ± s.d.). Stiffness during 10% shortening at  $V_0$  (Extended Data Fig. 2) was measured in fibres isolated from tibialis anterior muscles of adult male *Rana esculenta* at the Laboratory of Physiology (University of Florence, Italy), using the striation follower to monitor the half-sarcomere length change in response to step stretches in a segment near the force transducer end of the fibre.

Permeabilized muscle fibre segments were prepared from the psoas muscle of adult (~18 weeks old) male New Zealand white rabbits as described previously<sup>26</sup>. Bundles of 5–6 fibres, about 3–4 fibres wide and 1–2 fibres deep, were dissected on the day of the experiment and mounted horizontally in relaxing solution at ~2.4 µm sarcomere length between the lever arms of a strain gauge force transducer and a loudspeaker motor on a mechanical apparatus<sup>26</sup> modified for synchrotron X-ray experiments. Before each experiment, the ends of the bundle were fixed with glutaraldehyde and glued to aluminium foil clips with shellac dissolved in ethanol. Relaxing solution contained: 100 mM TES buffer, 7.7 mM MgCl<sub>2</sub>, 25 mM EGTA, 5.4 mM Na<sub>2</sub>ATP, 19.1 mM Na<sub>2</sub>-creatine phosphate (CP) and 10 mM reduced glutathione (GSH). Pre-activating solution contained: 100 mM TES, 6.9 mM MgCl<sub>2</sub>, 0.1 mM EGTA, 24.9 mM HDTA, 5.5 mM Na<sub>2</sub>ATP, 19.5 mM Na<sub>2</sub>CP and 10 mM GSH. Activating solution contained: 100 mM TES, 6.8 mM MgCl<sub>2</sub>, 25 mM CaEGTA, 5.5 mM Na<sub>2</sub>ATP, 19.5 mM Na<sub>2</sub>CP and 10 mM GSH. All solutions had 5 mM Mg-ATP; 1.2 mM free Mg<sup>2+</sup>; 199 mM ionic strength; pH 7.1 at 25 °C. Relaxing and activating solutions were mixed to obtain a series of partial activating solutions with the required free calcium ion concentrations. The osmotic agent dextran T500 (5% w/v) was added to all experimental solutions to reduce the interfilament spacing to a value similar to that of intact muscle (ref. 26 and references therein). The bundle was activated in a multidrop apparatus using a temperature-jump technique<sup>26</sup>; it was kept in pre-activating solution at low temperature (1 °C) for 2 min, then transferred to activating solution at 1 °C, in which little force was developed. When this force became steady (within 10 s) the bundle was transferred to activating solution at 25 °C and, following full force development, it was transferred to air for the X-ray exposure.

The investigators were not blinded to allocation during experiments and outcome assessment.

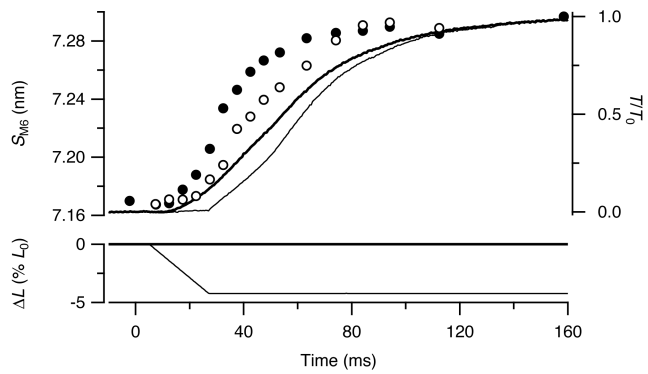
**X-ray data collection.** For intact fibres, the trough was sealed to prevent solution leakage, and the fibre was mounted vertically at beamline ID2 of the European Synchrotron Radiation Facility (ESRF)<sup>27</sup>, which provided up to  $2 \times 10^{13}$  photons per second at 0.1 nm wavelength in a beam of size ~300 µm (horizontal, full width at half-maximum (FWHM)) and ~100 µm (vertical) at the fibre. The beam was attenuated for fibre alignment. To minimize radiation damage, X-ray exposure was limited to the data collection period using a fast

electromagnetic shutter (nmLaser Products, Inc.) and the fibre was moved vertically by 100–200 µm between tetani. Data were collected from 50–80 tetani in each fibre with no detectable sign of radiation damage. X-ray diffraction patterns were recorded using the FReLoN charge-coupled device (CCD)-based detector with  $2,048 \times 2,048$  pixels binned by 16 in the horizontal direction and 2 in the vertical direction before the readout to increase the signal-to-noise ratio. Time frames of 3.5–6.5 ms were collected at rest, during 5%  $L_0$  steady shortening at  $V_0$  imposed 5 ms after the first stimulus, at the plateau of the isometric tetanus, during 5 or 10%  $L_0$  steady shortening at  $V_0$  imposed at the plateau of an isometric tetanus, and during force development following such shortening. The camera length was 10 m for recording the interference fine structure of the myosin-based M3 reflection and 3 m for recording the meridional reflections up to the M6. X-ray data are presented from ten fibres (five at 3 m and five at 10 m camera length, each fibre from a different frog) with a cross-sectional area of  $20,000 \pm 6,000$  µm<sup>2</sup> (mean ± s.d.) and isometric plateau force ( $T_0$ ) of  $254 \pm 90$  kPa.

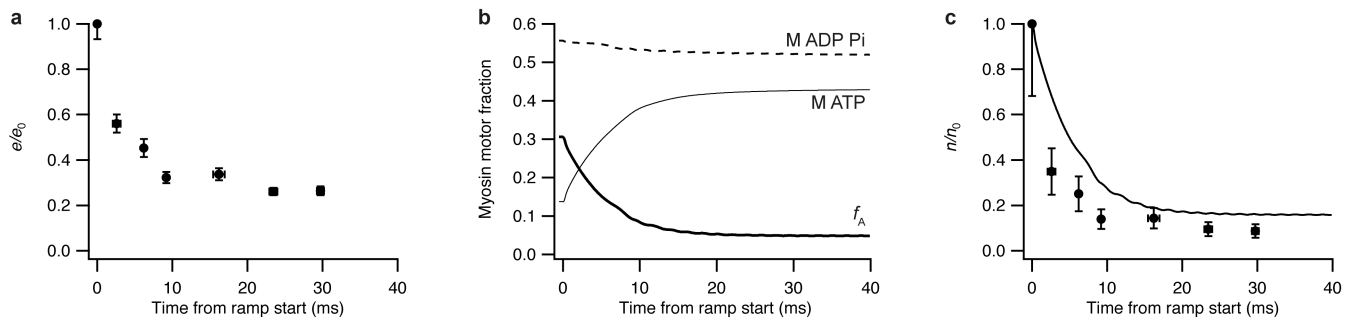
For X-ray experiments on permeabilized muscle fibres from rabbit psoas muscle, the multi-drop apparatus, which provided rapid solution exchange, temperature jumps and X-ray exposure in air, was mounted horizontally at the beamline. Data from 2–4 bundles were added for each point in Fig. 3d to increase the signal-to-noise ratio. Average bundle width was  $260 \pm 15$  µm; average fibre diameter was  $74 \pm 4$  µm (mean ± s.d.).

**X-ray data analysis.** X-ray diffraction data were analysed using the SAXS package (P. Boesecke, ESRF), Fit2D (A. Hammersley, ESRF) and IgorPro (WaveMetrics, Inc.). Two-dimensional patterns were centred and aligned using the equatorial 1,1 reflections, then mirrored horizontally and vertically. Data from fibres collected either at 10 m (2–5 fibres) or 3 m (2–5 fibres) were added together. The number of fibres was chosen in order to measure changes in relative intensities and spacings of the relevant X-ray reflections with adequate signal-to-noise; this could be achieved with a small number of fibres because the X-ray signals can be measured with extremely high precision and low biological variability<sup>3,8,9</sup>; for example, the spacing of the M6 reflection has an experimental standard deviation, including measurement and biological variability, of 0.005 nm (ref. 8), which is about 4% of the difference under investigation, between the resting state and  $T_0$ . The distribution of diffracted intensity along the meridional axis of the X-ray pattern (parallel to the fibre axis) was calculated by integrating from  $0.0046$  nm<sup>-1</sup> on either side of the meridian for the myosin-based M1 and M2 reflections,  $0.012$  nm<sup>-1</sup> for the M3 reflection and  $0.019$  nm<sup>-1</sup> for the M6 reflection. The first myosin layer line (ML1) was integrated in the region between  $0.064$  and  $0.037$  nm<sup>-1</sup> from the meridional axis. Background intensity distributions were fitted using a convex hull algorithm and subtracted; the small background remaining when the convex hull algorithm had been used was removed using the intensity from a nearby region of the X-ray pattern containing no reflections. Integrated intensities were obtained from the following axial regions: M1,  $0.021$ – $0.024$  nm<sup>-1</sup>; M2,  $0.046$ – $0.048$  nm<sup>-1</sup>; M3,  $0.067$ – $0.072$  nm<sup>-1</sup>; M6,  $0.133$ – $0.144$  nm<sup>-1</sup>; and ML1,  $0.019$ – $0.023$  nm<sup>-1</sup>. The limits for ML1 were chosen to exclude the contribution of the first actin layer line. The cross-meridional width of the M1, M2, M3 and M6 reflections was determined from the integrated intensity in a zone parallel to the equatorial axis in the axial regions specified above for the four reflections using a Gaussian fit across the meridian in the regions  $\pm 0.0037$  nm<sup>-1</sup>,  $\pm 0.0073$  nm<sup>-1</sup>,  $\pm 0.018$  nm<sup>-1</sup> and  $\pm 0.034$  nm<sup>-1</sup>, respectively. The interference components of the M3 reflection were determined by fitting multiple Gaussian peaks with the same axial width to the meridional intensity distribution, and the total intensity of the reflection was calculated as the sum of the component peaks. The spacing of each reflection was determined from the weighted mean of the component peaks, and calibrated using an M3 spacing of 14.34 nm in the resting fibre<sup>4</sup>. The combined instrumental point spread function was negligible compared with the radial width of the M3 reflection. Force, stimulus, sarcomere length, fibre length change and X-ray acquisition timing were collected and analysed using LabVIEW (National Instruments).

24. Huxley, A. F. & Lombardi, V. A sensitive force transducer with resonant frequency 50 kHz. *J. Physiol. (Lond.)* **305**, 15–6P (1980).
25. Huxley, A. F., Lombardi, V. & Peachey, L. D. A system for fast recording of longitudinal displacement of a striated muscle fibre. *J. Physiol. (Lond.)* **317**, 12P–13P (1981).
26. Linari, M., Caremani, M., Piperio, C., Brandt, P. & Lombardi, V. Stiffness and fraction of myosin motors responsible for active force in permeabilized muscle fibers from rabbit psoas. *Biophys. J.* **92**, 2476–2490 (2007).
27. Narayanan, T., Diat, O. & Boesecke, P. SAXS and USAXS on the high brilliance beamline at the ESRF. *Nucl. Instrum. Methods Phys. Res. Sect. A* **467–468**, 1005–1009 (2001).



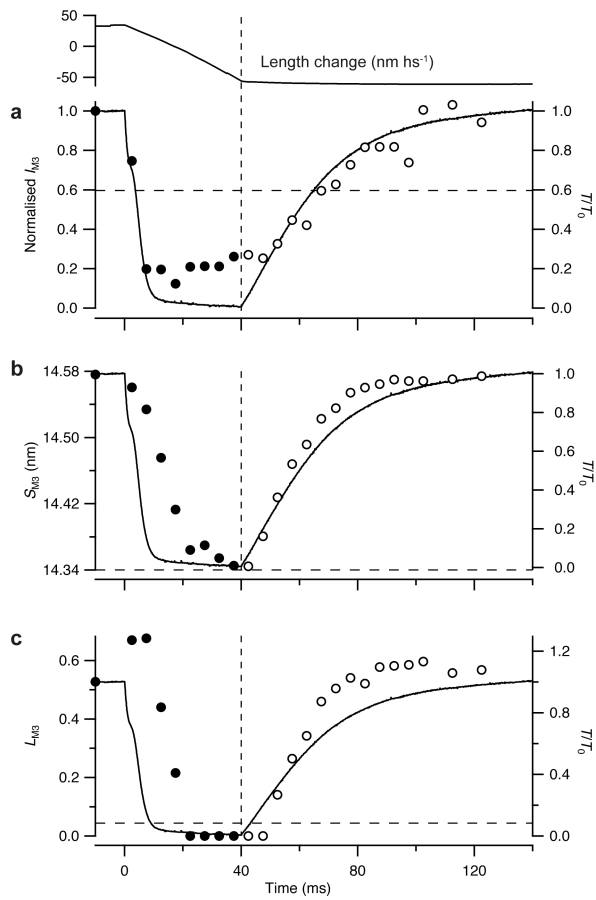
**Extended Data Figure 1 | The increase in the spacing of the M6 reflection on activation is delayed by imposing a period of unloaded shortening.** The top traces show  $S_{M6}$  (circles) superimposed on force (continuous line); filled/open circles and thicker/thinner line denote data from fixed-end tetani and tetani with imposed shortening, respectively. The bottom traces show imposed length change ( $\Delta L$ , expressed as percentage of initial fibre length (%  $L_0$ )). X-ray data added from one/two repeats of the protocol in three muscle fibres.



### Extended Data Figure 2 | Stiffness changes during unloaded shortening.

**a**, Half-sarcomere stiffness ( $e$ ) relative to that at the plateau of an isometric tetanus ( $e_0$ ), at different times after the start of unloaded shortening of 10%  $L_0$  applied at the tetanus plateau, calculated from the ratio of force and half-sarcomere length changes in response to 0.2%  $L_0$  step stretches complete in 100  $\mu$ s. Mean  $\pm$  s.e.m. from four fibres; species, *Rana esculenta*, 4 °C;  $e_0 = 0.27 \pm 0.01 T_0 \text{ nm}^{-1}$ ;  $T_0 = 137 \pm 13 \text{ kPa}$ . **b**, Fraction of myosin motors attached to actin ( $f_A$ ; thick solid line) and fractions with bound ATP (thin solid line) or ADP and inorganic phosphate ( $P_i$ ) (dashed

line) as a function of time during unloaded shortening, calculated from the kinetic model described in the Supplementary Discussion. **c**, Number of myosin motors attached to actin ( $n$ ) relative to that at the plateau of an isometric tetanus ( $n_0$ ), at different times during unloaded shortening, calculated from  $e/e_0$  in **a** as described in the Supplementary Discussion. Mean  $\pm$  s.e.m. from four fibres; s.e.m. includes the contribution of errors in measured values of filament and parallel elasticity. The thick line was calculated by normalizing  $f_A$  in **b** for its tetanus plateau value.



**Extended Data Figure 3 | Changes in the intensity, spacing and interference fine structure of the M3 reflection associated with a period of unloaded shortening.** Top, sarcomere length change in nanometres per half-sarcomere. **a–c**, Changes in intensity ( $I_{M3}$ ; **a**), spacing ( $S_{M3}$ ; **b**) and interference fine structure ( $L_{M3}$ ; **c**) (circles) superimposed on force (continuous line). Horizontal dashed lines, resting value of X-ray parameter; vertical dashed lines, time of end of shortening. X-ray data added from three fibres. Filled/open circles denote data before/after the end of shortening.